CONTROLLER DESIGN FOR THE ST7 DISTURBANCE REDUCTION SYSTEM

P. Maghami, F. L. Markley, C. J. Dennehy, M. B. Houghton
NASA Goddard Space Flight Center
Guidance, Navigation and Control Division
Greenbelt, MD 20771

William M. Folkner
Jet Propulsion Laboratory
California Institute of Technology
Pasadena, CA 91109

Abstract

The Space Technology 7 experiment will perform an on-orbit system-level validation of two specific Disturbance Reduction System technologies: a gravitational reference sensor employing a free-floating test mass and a set of micro-Newton colloidal thrusters. The Disturbance Reduction System is designed to maintain a spacecraft's position with respect to the free-floating test mass to less than 10 nm/√Hz, over the frequency range 10^{-3} Hz to 10^{-2} Hz. This paper presents the design and analysis of the coupled drag-free and attitude control system that closes the loop between the gravitational reference sensor and the micro-Newton thrusters while incorporating star tracker data at low frequencies. The effects of actuation and measurement noise and disturbances on the spacecraft and test masses are evaluated in a seven-degree-of-freedom planar model incorporating two translational and one rotational degrees of freedom for the spacecraft and two translational degrees of freedom for each test mass.

Introduction

NASA's New Millennium Program (NMP) recently selected the Disturbance Reduction System (DRS) flight validation experiment, managed by the Jet Propulsion Laboratory (JPL), for the Space Technology 7 (ST7) mission [1]. NMP missions are intended to validate advanced technologies that have not flown in space in order to reduce the risk of their infusion in future NASA Space Science missions. The ST7 DRS incorporates two specific technologies: a highly sensitive Gravitational Reference Sensor (GRS), provided by Stanford University, to measure the position and attitude of a spacecraft with respect to an internal free-floating test mass, and a set of micro-Newton colloidal thrusters, provided by the Busek Company. The ST7 DRS, scheduled to fly on the European Space Agency's SMART-II spacecraft in 2006, is designed to maintain the spacecraft's position, with respect to the GRS free-floating test mass, to less than 10 nm/√Hz, over ST7's science measurement frequency range from 1 to 10 mHz.

This paper presents the overall design and analysis process of the spacecraft controller being developed at NASA's Goddard Space Flight Center to close the loop between the GRS and the micro-Newton colloidal thrusters. A two-dimensional planar model has been developed to capture the essential dynamics of the ST7-DRS package. It includes seven rigid-body dynamic degrees of freedom: two translations and a rotation for the spacecraft, and two translations for each test mass, ignoring the inessential rotational dynamics of the test masses. Actuation and measurement noise and disturbance sources acting on the spacecraft and test masses are modeled. The ST7 DRS comprises three control systems: the attitude control system (ACS) to maintain a sun-pointing attitude; the drag free control (DFC) to center the spacecraft about the test masses; and the test mass suspension control. This paper summarizes the control design and analysis of the ST7-DRS 7-DOF model.

Model Description

The configuration used for the current 7-DOF Model is shown in Figure 1. Here the location and the orientation of the two test masses can be arbitrarily assigned. The nominal position vectors for the two test masses and their respective housings are chosen as $\mathbf{R}_1 = [0.1 \quad 0]^t$ m and $\mathbf{R}_2 = [0.3 \quad 0]^t$ m, which means that the sensitive axis is along the X-axis of the spacecraft. Two clusters, each containing two thrusters, are located on the ±X faces to provide thrust capability for attitude and drag-free control. It should be pointed out that in the current analysis the thruster configurations are mainly used for thrust noise characterization. Thrust commands for attitude control and drag-free control are assumed in the

spacecraft body frame, and are not resolved to the individual thrusters. Two disturbances are included in this model. The first is the nominal solar radiation pressure and its variation. The Sun exposed face of the spacecraft corresponds to the –Y direction. The angle of the incident rays of the sun to the surface normal, α, may be arbitrarily assigned. However, it is assumed to be zero for the current analysis. The frequency spectrum used for solar radiation flux variations is given in Figure 2. This spectrum was based on refs. [2] and [3], and represents a conservative assessment of potential variations. This plot indicates a constant spectrum at the frequencies below 0.1 mHz, followed by a $1/f$ roll off. This spectrum also includes the so-called 5-minute acoustic oscillation (at 3.5 mHz), and levels off at frequencies above 10 mHz. The second disturbance source modeled was the acceleration noise on the test mass. A number of sources contribute to this acceleration noise, including magnetic and Lorentz forces, thermal disturbances, cosmic ray impacts, etc [2]. The spectral density function for the test mass acceleration noise is assumed to have the following characteristics:

- $1/f^2$ rolloff at frequency range of 0.01-0.1 mHz,
- $1/f$ rolloff at frequency range of 0.1-1 mHz,
- constant $3\text{x}10^{-14}$ m/s^2/Hz$^{0.5}$ at frequencies above 1 mHz.

In order to incorporate this power spectrum within the frequency and time domain analyses, the linear filter approximation shown in Figure 3 was developed. Note that all requirements are either met or exceeded by this approximation. It should be noted that the acceleration noise was applied to both test masses in all directions.

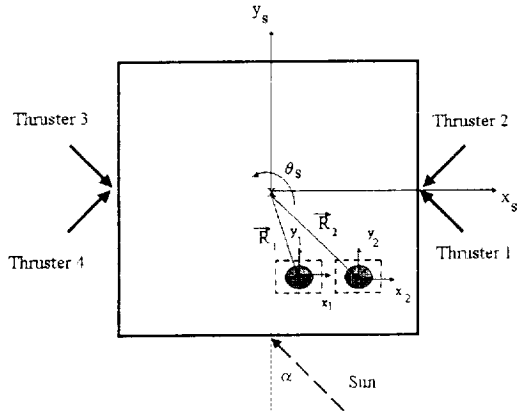

Figure 1 7-DOF Model Configuration

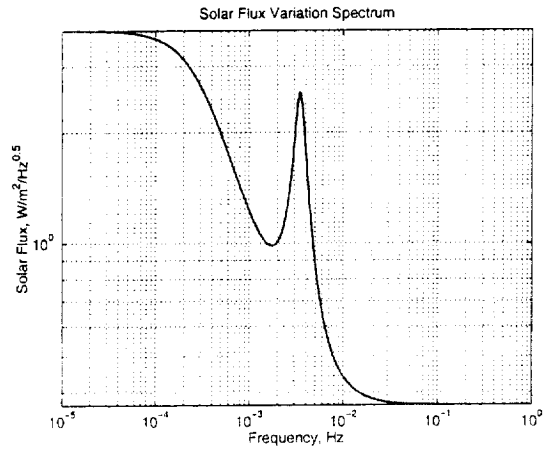

Figure 2 Root Power Spectrum of the Solar Radiation Flux Variations

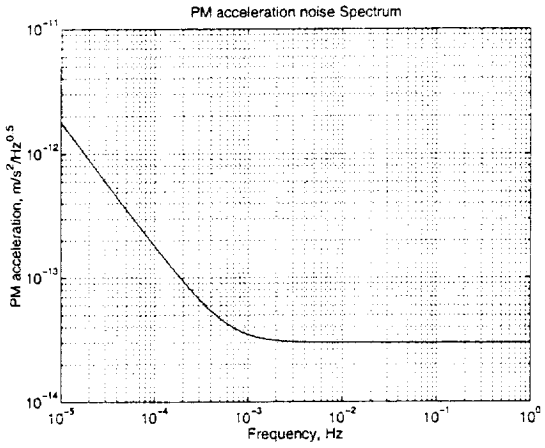

Figure 3 Root Power Spectrum for the Test Mass Acceleration Noise

White-noise models were used to capture thruster noise, electrostatic suspension force noise, star tracker noise, and the capacitive sensing noise (used to measure the relative positions of the teat masses in the spacecraft). The intensity levels are captured in Table 1.

Table 1 Actuation and Sensing Noise Intensities

Noise Source	Intensity
Thrusters	0.1 μN/Hz$^{0.5}$
Suspension Force	2e-14 N/Hz$^{0.5}$
Star Tracker	10 arcsec/ Hz$^{0.5}$
Capacitive Sensing	3 nano-m/ Hz$^{0.5}$

Controller Design

A top-level block diagram of the system dynamics is shown in Figure 4. Here there are five output measurements used by the control system: the relative positions of test mass 1 in X and Y; the relative positions of test mass 2 in X and Y; and the spacecraft attitude error from the star tracker. The five control inputs are thruster force commands in X and Y, thruster torque command, and the suspension control force commands on test mass 2 in X and Y. It is important to note that no suspension forces are applied to test mass 1. There are two main control loops required for the spacecraft control. First is the drag-free controller, which controls the position of the spacecraft (in X and Y) to establish the drag-free motion of test mass 1. The second controller is the spacecraft attitude control, which is primarily designed to orient the spacecraft in the low frequency band (DC and near DC) using the star tracker data. However, it is also designed to center the spacecraft about test mass 2 and thus to establish drag-free conditions for both test masses simultaneously in the ST7 science measurement band from 1 to 10 mHz.

The drag-free controller, which includes two loops (one for X-axis control and one for Y-axis control), was designed using a classical control approach. However, in this model, the relative test mass positions, which are used by the drag free controller, are not only a function of the spacecraft and test mass translations, but also are affected by the attitude of the spacecraft. The drag-free controller was a Proportional-Integral-Derivative (PID) controller with a roll-off filter.

$$\begin{aligned} u_x(s) &= K_d(s)x_1(s) \\ u_y(s) &= K_d(s)y_1(s) \end{aligned} \tag{1}$$

$$K_d(s) = [G_{pd} + sG_{dd} + \frac{G_{id}}{s}]F_d(s) \tag{2}$$

where $x_1(s)$ and $y_1(s)$ denote the measured relative position of test mass 1 from its caging in X and Y, respectively. The terms $u_x(s)$ and $u_y(s)$ denote the required control thrust force in X and Y. G_{pd}, G_{dd}, and G_{id} denote the proportional, derivative, and integral gains. The term $F_d(s)$ denotes the third-order attenuation filter. The current drag-free controller is defined as

$$K_d(s) = \frac{2811\,s^2 + 634.9\,s + 13.36}{s^4 + 5.969\,s^3 + 17.81\,s^2 + 26.58\,s} \tag{3}$$

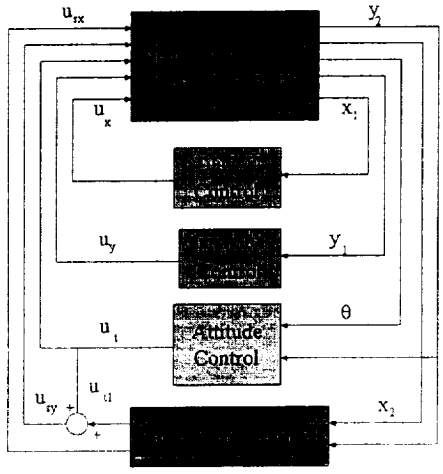

Figure 4 Block Diagram of the 7-DOF System

This controller provides a cut-off frequency of 0.055 Hz. It should be noted that all sensor measurements are updated at 10 Hz sampling with the exception of the star tracker signal, which is updated at 1 Hz. Moreover, approximations to zero-order hold and expected computational/transport delays, in the form of a Pade approximation, were included in the plant dynamics.

The attitude controller is a two-input/single-output controller, which uses star tracker measurements and the relative position of test mass 2 in the Y-direction as inputs. This controller was designed following a classical design approach and uses blending filters to accommodate its two tasks. The structure of the attitude control may be summarized as follows.

$$u_t(s) = K_{al}(s)\theta(s) + K_{ah}(s)y_2(s) \tag{4}$$

Here $\theta(s)$ denotes the attitude error measurement obtained from the star tracker data, $y_2(s)$ represents the measured relative position of test mass 2 from its caging in the Y-direction, and $u_t(s)$ denotes the required thrust control torque. The term $K_{al}(s)$ denotes the low-bandwidth part of the attitude control designed to maintain the attitude of the spacecraft. Its design is a classical PID loop with an appropriate roll-off filter, given as

$$K_{al}(s) = \frac{b_1\,s^4 + b_2 s^3 + b_3 s^2 + b_4 s + b_5}{s^5 + a_1 s^4 + a_2 s^3 + a_3 s^2 + a_4 s + a_5} \tag{5}$$

$$a_1 = 0.008209 \quad b_1 = 1.625e-21$$
$$a_2 = 3.37e-5 \quad b_2 = 1.378e-24$$
$$a_3 = 8.102e-8 \quad b_3 = 7.497e-12$$
$$a_4 = 9.741e-11 \quad b_4 = 1.682e-15$$
$$a_5 = 0 \quad b_5 = 2.246e-19$$

This controller provides a cut-off frequency of about 0.00005 Hz. The controller term $K_{ah}(s)$ represents the part of the attitude controller that centers the spacecraft about test mass 2 in the transverse direction (Y-direction) in the ST7-DRS measurement band. This controller is also designed based on the classical approach, and is a series combination of lead-lag filter, PD filter, and a roll-off filter, resulting in a sixth-order controller with the following transfer function.

$$K_{ah}(s) = \frac{b_1 s^5 + b_2 s^4 + b_3 s^3 + b_4 s^2 + b_5 s + b_6}{s^6 + a_1 s^5 + a_2 s^4 + a_3 s^3 + a_4 s^2 + a_5 s + a_6} \quad (6)$$

$$a_1 = 3.579 \quad b_1 = 388.9$$
$$a_2 = 6.406 \quad b_2 = 70.8$$
$$a_3 = 0.1596 \quad b_3 = 0.1764$$
$$a_4 = 0.0015 \quad b_4 = 0.0001658$$
$$a_5 = 6.273e-06 \quad b_5 = 6.934e-08$$
$$a_6 = 9.845e-09 \quad b_6 = 1.088e-11$$

The relative X and Y position of test mass 2 is controlled by the electrostatic suspension control internal to the GRS. The relative position in X is controlled via a low bandwidth PID controller to provide disturbance rejection at DC and near DC. The Y-position control comprises two compensators. One is a low bandwidth PID controller to provide disturbance rejection at DC and near DC. The other is a feedforward compensator that nulls out the compensation effects of the low bandwidth attitude controller. This compensation removes a significant part of the coupling between the attitude loop and the 2nd test mass position control in Y, and therefore makes the system more amenable to decentralized control. It also naturally corrects for any disturbances caused in the test mass position control loop by attitude control commands. The structure of this controller is given by

$$u_{sy}(s) = K_{sy}(s) y_2(s) + h * K_{al}(s)\theta(s) \quad (7)$$

Here $u_{sy}(s)$ denotes the suspension control force for test mass 2 in Y. The nominal controller, $K_{sy}(s)$, is a low-bandwidth PID loop, and the scaling constant h depends on the moment arm from spacecraft center of mass to the test mass, the spacecraft inertia, and the mass of the test mass.

Stability Margins

Each of the controllers was designed to have sufficient stability margins. However the 7-DOF system represented in Figure 4 is a MIMO system, by virtue of the cross coupling between the relative test mass positions and the attitude of the spacecraft. Hence, the loop gains at each input and output channel (while the remaining channels are closed) must be analyzed to obtain proper stability margins. The stability analysis indicates that each input/output channel has at least 8 dB of gain margin and 36° of phase margin. These margins are amply sufficient considering that the effects of zero-order hold and computational and transport delay dynamics are already included in the analysis. Figure 5 illustrates the loop gain for the relative position of test mass 1 in the X direction, while Figure 6 provides the same for the Y-axis suspension force.

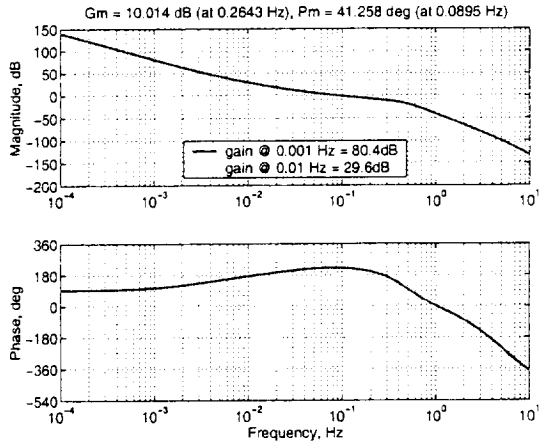

Figure 5 Loop Gain at the Relative Position of Test Mass 1: X-Direction

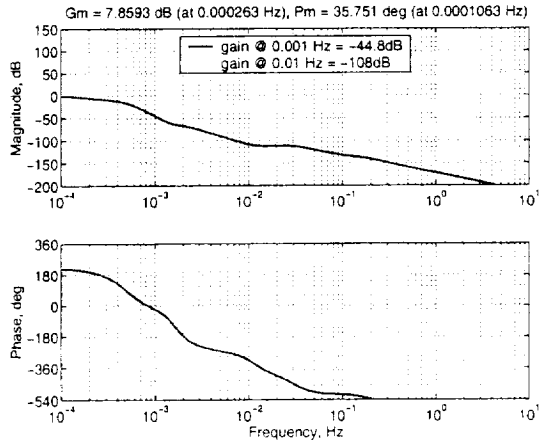

Figure 6 Loop Gain at the Y-axis Suspension Force

Analysis Results

The attitude and drag-free controllers were implemented within a MATLAB-based model of the system that serves as the design and analysis tool for the 7-DOF Model. Both time-domain and frequency-domain analyses were performed. The results of the frequency-domain analyses are shown in Figures 7–16. Figures 7 and 8 illustrate the root power spectral densities of the relative positions of test mass 1, in both X and Y directions, for various disturbance and noise sources. The plots in each disturbance category represent the root sum squared (RSS) values for that category; for example, the thruster noise plot is the RSS contribution of the noise from all four thrusters. The RSS of all spectra is mainly dominated by the thruster noise and measurement noise. The cross coupling that exists in this MIMO system may be observed in the variations in the contributions from different thruster noise sources, as well as the contribution of solar radiation pressure noise in the X direction. Figures 9 and 10 shows the root power spectral densities of the relative positions of test mass 2. Both test masses satisfy the positioning requirement of 10 nm/$\sqrt{}$(Hz) in both directions in the science measurement band, although the spacecraft only follows test mass 1 and the position of test mass 2 is not controlled in X in the science measurement band. The main contributions come from the acceleration noise on the two test masses and the thruster noise. Figure 11 shows the root spectrum for the spacecraft pointing error, which indicates that the error is well within its requirement of 1°/$\sqrt{}$(Hz). Figures 12 and 13 illustrate the spectra for the thruster force command in X and Y directions, respectively; the RSS levels are well within the 20 μN capability of the colloidal thrusters. Figure 14 shows the root spectrum for the thrust torque commands. Figures 15–16 illustrate spectrum of the suspension control forces on test mass 2 in X and Y directions, respectively; these are well within the requirement of 10 nN/$\sqrt{}$(Hz).

Figures 17 and 18 illustrate typical time-domain analysis results, the time history responses of the relative positions of the two test masses in the X-direction. It can be seen from Figure 17 that the displacement of proof mass 1 never exceeds 4 nm, and only very occasionally exceeds 3 nm, in agreement with the frequency domain results of Figure 7. Figure 18 shows that the low bandwidth position control of test mass 2 results in a very long system time constant, so it takes significant time for the relative position to reach its steady-state values. This slow response, which also holds true for the spacecraft attitude error, will be addressed by carefully managing the transition from using the GRS in accelerometer mode to drag-free control in the fully-developed DRS. The lower plot in Figure 17 shows a 1000 second snapshot of the time history (from 149000s to 150000s), which shows acceptable steady-state behavior.

Discussion

It is concluded from time-domain and frequency-domain analyses that all the requirements for the ST7-DRS control systems are met in a planar seven-degree-of-freedom model. These include establishing drag-free motion of the test masses in the science band as well as spacecraft attitude control. The spacecraft position relative to the primary test mass will be maintained within the required precise limits. It was also proved possible to electrostatically suspend the second test mass while maintaining its drag-free state within the frequency range of interest, by rapidly rolling off of the X axis suspension forces between DC and the measurement frequency band. Successful spacecraft attitude control is accomplished by combining low frequency data from a star tracker and high frequency data from the transverse position of the second test mass. All these conclusions must be confirmed in a three-dimensional sixteen-degree-of-freedom dynamic model of the spacecraft and test masses. No essential complications are expected to arise at this level, however.

References

[1] Keiser, G. M., Buchman, S., Byer, R. L., Folkner, W. M., Hruby, V., and Gamero-Castaño, M., "Disturbance Reduction System for Testing Technology for Drag-Free Operation," SPIE Paper 4856-02, Astronomical Telescopes and Instrumentation Conference, Waikoloa, Hawaii, USA, August 2002.

[2] Final Technical Report of the (Phase A) Study of the Laser Interferometer Space Antenna (Dornier Satellintensysteme GmbH – Matra Marconi Space – Alenia Aerospzio) ESTEC Contract no. 13631/99/NL/MS, Report No. LI-RP-DS-009, April 2000

[3] J. Pap, et. al., "Variation in Total Solar and Spectral Irradiance as Measured by the VIRGO Experiment on SOHO", *Adv. Space Res.*, 24:215-224, 1999.

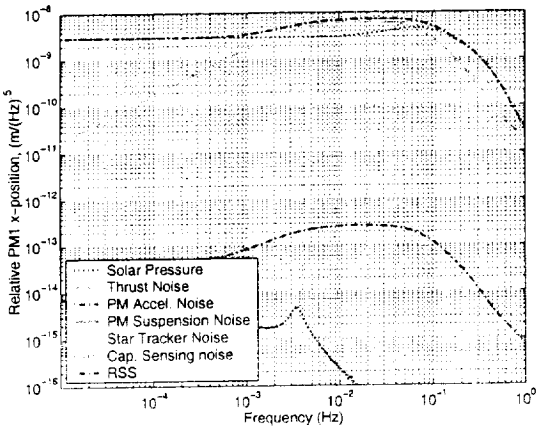

Figure 7 Root Power Spectrum of the Relative Position of Test Mass 1: X-direction

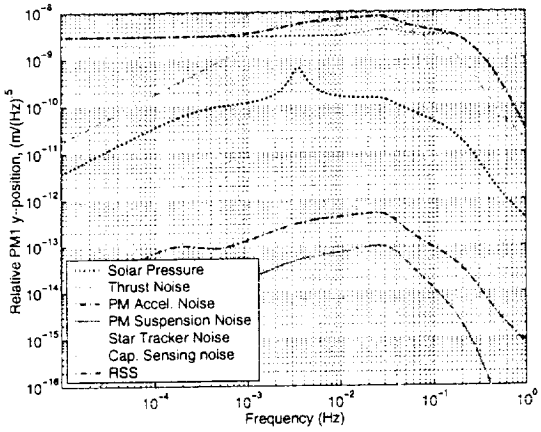

Figure 8 Root Power Spectrum of the Relative Position of Test Mass 1: Y-direction

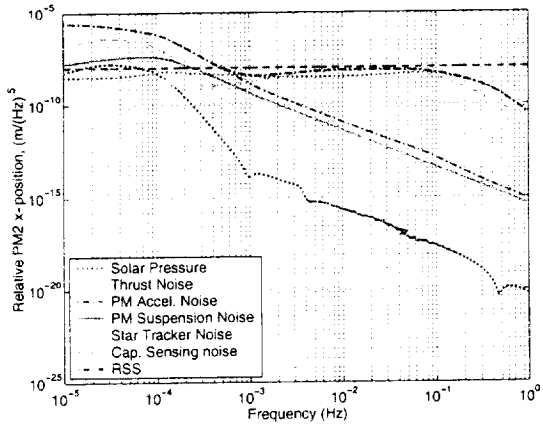

Figure 9 Root Power Spectrum of the Relative Position of Test Mass 2: X-Direction

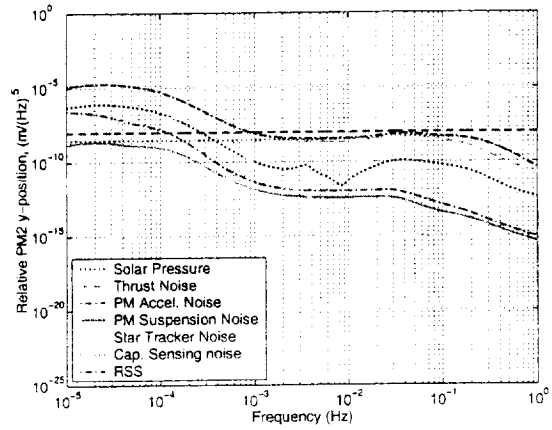

Figure 10 Root Power Spectrum of the Relative Position of Test Mass 2: Y-direction

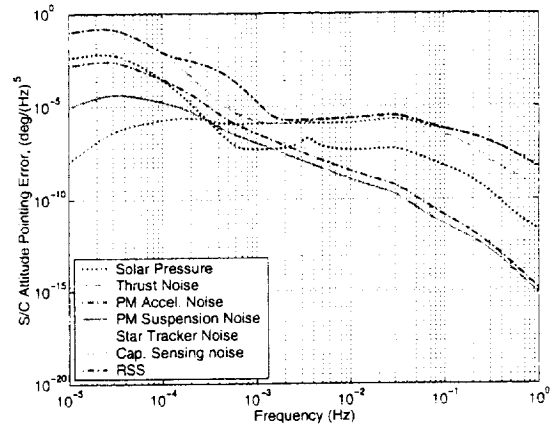

Figure 11 Root Power Spectrum of the Spacecraft Attitude Pointing Error

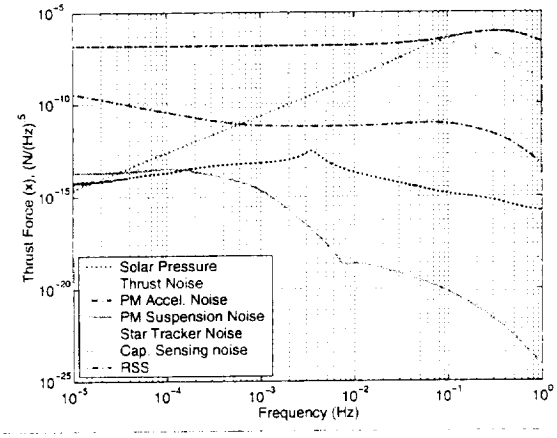

Figure 12 Root Power Spectrum of the Thrust Force: X-direction

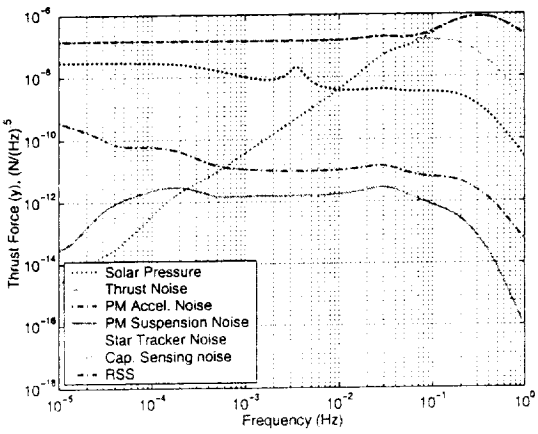

Figure 13 Root Power Spectrum of the Thrust Force: Y-direction

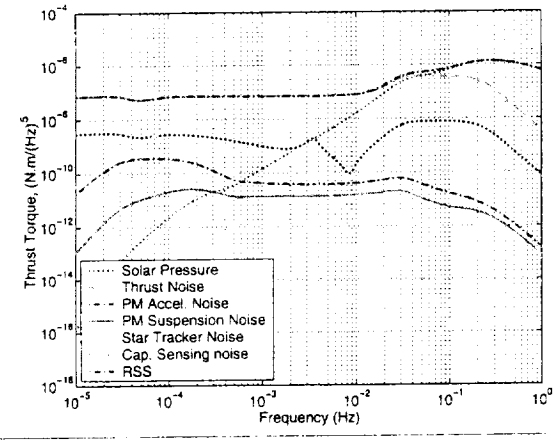

Figure 14 Root Power Spectrum of the Thrust Torque

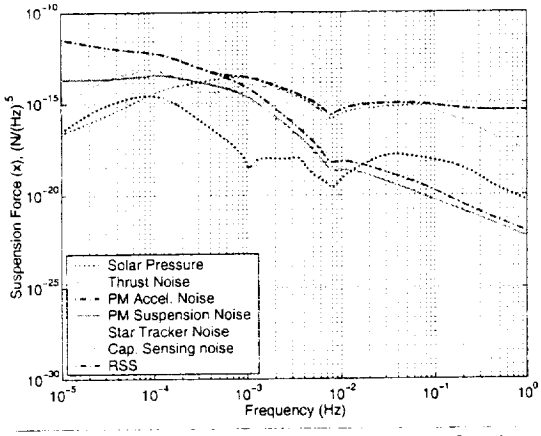

Figure 15 Root Power Spectrum of the X-axis Suspension Force

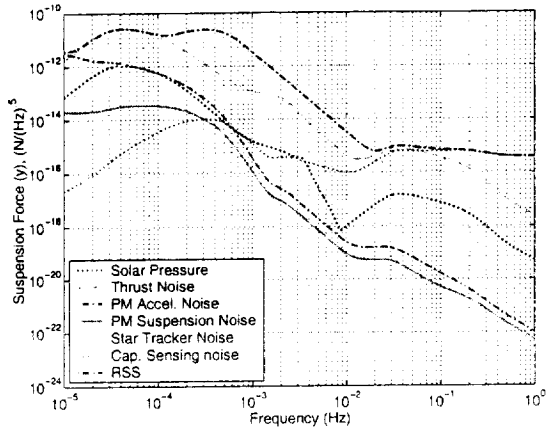

Figure 16 Root Power Spectrum of the Y-axis Suspension Force

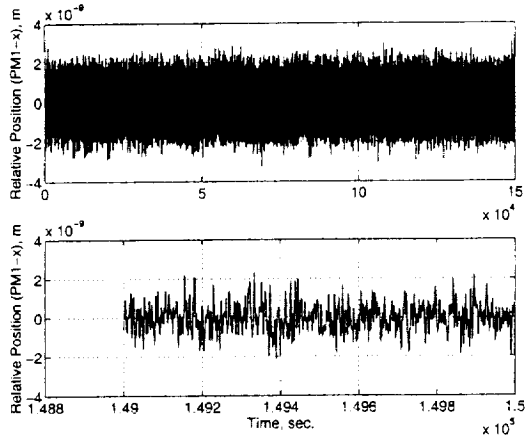

Figure 17 Time History for the Relative Position of Test Mass 1: X-Direction

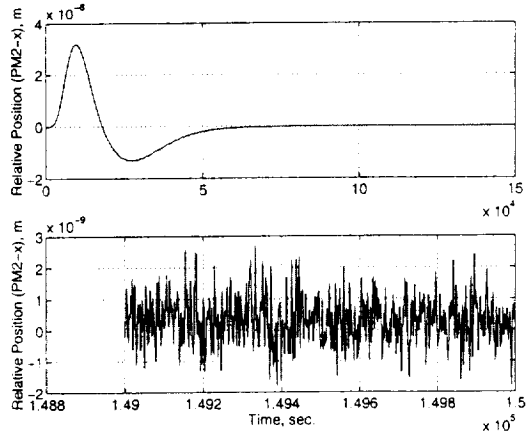

Figure 18 Time History for the Relative Position of Test Mass 2: X-Direction